JACS
JOURNAL OF THE AMERICAN CHEMICAL SOCIETY

Subscriber access provided by ISTANBUL TEKNIK UNIV

Article

Anion-Induced Adsorption of Ferrocenated Nanoparticles

Rebecca L. Stiles, Ramjee Balasubramanian, Stephen W. Feldberg, and Royce W. Murray

J. Am. Chem. Soc., **2008**, 130 (6), 1856-1865 • DOI: 10.1021/ja074161f

Downloaded from http://pubs.acs.org on February 8, 2009

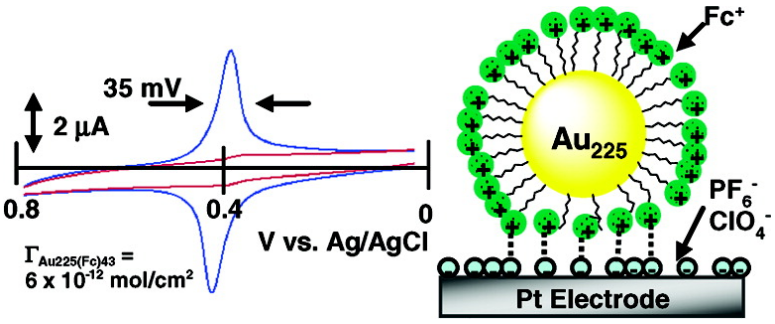

More About This Article

Additional resources and features associated with this article are available within the HTML version:

- Supporting Information
- Links to the 1 articles that cite this article, as of the time of this article download
- Access to high resolution figures
- Links to articles and content related to this article
- Copyright permission to reproduce figures and/or text from this article

View the Full Text HTML

ACS Publications
High quality. High impact.

Journal of the American Chemical Society is published by the American Chemical Society. 1155 Sixteenth Street N.W., Washington, DC 20036

J|A|C|S
ARTICLES
Published on Web 01/17/2008

Anion-Induced Adsorption of Ferrocenated Nanoparticles

Rebecca L. Stiles,[†] Ramjee Balasubramanian,[†] Stephen W. Feldberg,[‡] and Royce W. Murray*,[†]

Kenan Laboratories of Chemistry, University of North Carolina, Chapel Hill, North Carolina 27599, and Chemistry Department, Brookhaven National Laboratory, Upton, New York 11973

Received June 7, 2007; E-mail: rwm@email.unc.edu

Abstract: Au nanoparticles fully coated with ω-ferrocenyl hexanethiolate ligands, with average composition Au_{225}(ω-ferrocenyl hexanethiolate)$_{43}$, exhibit a unique combination of adsorption properties on Pt electrodes. The adsorbed layer is so robust that electrodes bearing submonolayer, monolayer, and multilayer quantities of these nanoparticles can be transferred to fresh electrolyte solutions and there exhibit stable ferrocene voltammetry over long periods of time. The kinetics of forming the robustly adsorbed layer are slow; monolayer and submonolayer deposition can be described by a rate law that is first order in nanoparticle concentration and in available electrode surface. The adsorption mechanism is proposed to involve entropically enhanced (multiple) ion-pair bridges between oxidized (ferrocenium) sites and certain specifically adsorbed electrolyte anions on the electrode. Adsorption is promoted by scanning to positive potentials (through the ferrocene wave) and by high concentrations of $Bu_4N^+X^-$ electrolyte ($X^- = ClO_4^-$, PF_6^-) in the CH_2Cl_2 solvent; there is no adsorption if X^- = *p*-toluenesulfonate or if the electrode is coated with an alkanethiolate monolayer. The electrode double layer capacity is not appreciably diminished by the adsorbed ferrocenated nanoparticles, which are gradually desorbed by scanning to potentials more negative than the electrode's potential of zero charge. At very slow scan rates, voltammetric current peaks are symmetrical and nearly reversible, but exhibit E_{fwhm} considerably narrower (typically 35 mV) than ideally expected (90.6 mV, at 298 K) for a one-electron transfer or for reactions of multiple, independent redox centers with identical formal potentials. The peak narrowing is qualitatively explicable by a surface-activity effect invoking large, attractive lateral interactions between nanoparticles and, or alternatively, by a model in which ferrocene sites react serially at formal potentials that become successively altered as ion-pair bridges are formed. At faster scan rates, both ΔE_{peak} and E_{fwhm} increase in a manner consistent with a combination of uncompensated ohmic resistance of the electrolyte solution and of the adsorbed film, as distinct from behavior produced by slow electron transfer.

Introduction

Adsorption of ions and molecules from solutions onto electrodes and electrified interfaces is a common chemical phenomenon. During a study[1] of the electrochemistry of Au nanoparticles capped with monolayers of solely ferrocene alkanethiolate ligands (monolayer protected clusters, MPCs), we noticed an uncommon result—a nearly irreversible adsorption of a ca. monolayer of ω-ferrocenyl hexanethiolate-functionalized MPCs from CH_2Cl_2 solutions onto Pt electrodes. Further study of this adsorption has been carried out and the present report will show that the adsorption of the MPC ($Au_{225}[(S(CH_2)_6Fc)_{43}]$) is a slow, cooperative process, requiring the presence of high concentrations of particular electrolytes.

While studying the adsorption of the ferrocenated MPCs, several unusual properties of the electroactive film were discovered. First, the monolayer is robust, persisting after rinsing, soaking, or sonication of the electrode in solvent (with or without dissolved electrolyte). After transferring the filmed electrode to a nanoparticle-free CH_2Cl_2 electrolyte solution, well-defined stable voltammetry of the ferrocene ligands (*ca.* 43 per nanoparticle) can be observed. The full-width-half-maximum (E_{fwhm}) of the voltammetric peak (for monolayer and submonolayer coverage, ca. 35 mV) is considerably narrower than the value expected (90.6 mV at 298 K) for an electroactive monolayer. Analysis of anodic/cathodic peak potential separations (ΔE_{peak}) reveals an uncompensated ohmic resistance of the adsorbed MPC layer, while the electrode's double layer capacitance remains virtually unchanged. The adsorbed layer is slowly removed by applying potentials estimated to be more negative than the electrode's potential of zero charge, and the adsorption is nearly completely blocked by the prior formation of a dodecanethiolate self-assembled monolayer. This paper will analyze these collectively unusual effects.

The charge under the peaks of a cyclic voltammogram of an electroactive film on an electrode, that is, a chemically modified electrode,[2−9] gives the total surface coverage, Γ_T (mol/cm^2).

[†] University of North Carolina.
[‡] Brookhaven National Laboratory.

(1) Wolfe, R. L.; Balasubramanian, R.; Tracy, J. B.; Murray, R. W. *Langmuir* **2007**, *23*, 2247−2254.
(2) Chidsey, C. E. D.; Murray, R. W. *Science* **1986**, *231*, 25−31.
(3) Murray, R. W.; Ewing, A. G.; Durst, R. A. *Anal. Chem.* **1987**, *59*, A379.
(4) Wrighton, M. S. *Science* **1986**, *231*, 32−37.
(5) Faulkner, L. R. *Chem. Eng. News* **1984**, *62*, 28.
(6) Murray, R. W. *Electroanal. Chem.* **1984**, *13*, 191−368.

10.1021/ja074161f CCC: $40.75 © 2008 American Chemical Society

Many adsorbed species display near-ideal behavior, but reactions with slow monolayer electron-transfer kinetics are also known,[10−12] as are unusual voltammetric waveshapes attributed to nonideal surface activities and lateral interactions,[13−15] environmental or dipolar heterogeneity of redox sites,[16−18] ion-pairing between redox species and electrolyte counterions,[19,20] and interfacial potential distribution.[21] In the particular case of ferrocene, there are examples of adsorption from solutions that are either concentrated[22,23] or involve a poorly solvating medium (aqueous),[24] adsorption of ferrocenated dendrimers,[25] precipitation of poly(vinylferrocenium),[15,26−29] electrodeposition of biferrocene derivative-attached gold nanoparticles,[30−35] and binding through alkanethiolate[16] or siloxane linkages.[16,36] Among all these reports, however, there is none of a slow, electrolyte-induced, irreversible adsorption of monolayer quantities of a ferrocenated species that yield voltammetric surface waves more narrow than the ideal $E_{fwhm} = 90.6$ mV.

The Au MPCs used in these experiments have an average Au_{225}(ω-ferrocenyl hexanethiolate)$_{43}$ composition and are one of a series[1] of MPCs having average 75, 140, 225 and 314 Au atom core sizes and *ca.* 37, 39, 43 and 48 ferrocenyl ligands, respectively. Their non-ferrocenated analogues display size-dependent voltammetry with quantized one-electron double layer charging[37−47] for the three larger cores and a molecule-like energy gap[43] for the Au_{75} case. However, for the ferrocenated nanoparticles, the currents associated with the quantized charging are dwarfed by the much larger and more quantitatively definable currents associated with the oxidation or reduction of the multiple (ca. 43) ferrocene sites in the protecting monolayer surrounding each Au_{225} core. We focus on the latter currents in this study of ferrocenated MPC adsorption, which has also lead us to a further study[48] conducted in light of the implied possibilities of pseudocapacitive charge (energy) storage. Indeed, we find that analogous adsorption occurs on glassy and mesoporous carbon electrode materials. Additionally, provided the ion-induced adsorption mechanism can be extended to other nanoparticles (redox coated or not), it may be useful for their immobilization and formation of modified surfaces.

The ferrocenated nanoparticles referred to in the paper are fully (solely) capped with ω-ferrocenyl hexanethiolate ligands and are abbreviated $Au_{225}(SC6Fc)_{43}$. In one instance, these ligands are diluted with hexanethiolate ligands.

Experimental

Chemicals. Hexanethiol (HSC6, >99%), dodecanethiol (HSC12, >99%), *t*-octylammonium bromide (Oct_4NBr, >98%), sodium borohydride ($NaBH_4$, >98%), *t*-butylammonium perchlorate (Bu_4NClO_4, >99%), *t*-butylammonium *p*-toluenesulfonate ($Bu_4NC_7H_7SO_3$, puress), and *t*-butylammonium hexafluorophosphate (Bu_4NPF_6, puress) from Aldrich and toluene (reagent grade), acetonitrile (Optima), methylene chloride (HPLC grade), tetrahydrofuran (HPLC grade), and ethanol (HPLC grade) from Fisher were used as received. $HAuCl_4 \cdot xH_2O$ (from 99.999% pure gold) was synthesized using a literature procedure[49] and stored in a freezer at −20 °C. Water was purified using a Barnstead NANOpure system (18 MΩ).

Ferrocene hexanethiol (HSC6Fc) was synthesized by refluxing a mixture of (1.11 g, 3.17 mmol) ω-bromohexane ferrocene (prepared by a published method[50]) and thiourea (0.600 g, 7.88 mmol) in ethanol (50 mL) overnight. The reaction mixture was neutralized with NaOH (aq), refluxed for a further 3 h, and then acidified with HCl to pH ≈ 2, diluted with water, and extracted with CH_2Cl_2, washing the organic extract phase copiously with water. The material obtained after rotary evaporation of the CH_2Cl_2 product solution was chromatographed on silica gel with ethyl acetate/hexanes. ^{1}H NMR (400 MHz, CD_2Cl_2) of the thiol gave the appropriate NMR peaks: $\delta = 4.0$ (m, 9 H), 2.49 (q, $J = 7.2$ Hz, 2 H), 2.30 (t, $J = 7.6$ Hz, 2 H), 1.56 (m, 2 H), 1.46 (m, 2 H), and 1.32 (m, 5 H) ppm with no dithiol peaks present and no significant broadening, indicating that the majority of the ferrocenyl groups were in the reduced state.

MPC Synthesis. $Au_{225}(SC6Fc)_{43}$ was synthesized as previously described.[1] Briefly, vigorous mixing of 3.19 g $HAuCl_4 \cdot xH_2O$ in 100

(7) Murray, R. W. *Acc. Chem. Res.* **1980**, *13*, 135−141.
(8) Bard, A. J. *J. Chem. Educ.* **1983**, *60*, 302−304.
(9) Bard, A. J.; Faulkner, L. R. *Electrochemical Methods: Fundamentals and Applications*, 2nd ed.; Wiley: New York, 2001.
(10) Li, J. H.; Schuler, K.; Creager, S. E. *J. Electrochem. Soc.* **2000**, *147*, 4584−4588.
(11) Brevnov, D. A.; Finklea, H. O. *J. Electrochem. Soc.* **2000**, *147*, 3461−3466.
(12) Creager, S. E.; Wooster, T. T. *Anal. Chem.* **1998**, *70*, 4257−4263.
(13) Matsuda, H.; Aoki, K.; Tokuda, K. *J. Electroanal. Chem.* **1987**, *217*, 15−32.
(14) Brown, A. P.; Anson, F. C. *Anal. Chem.* **1977**, *49*, 1589−1595.
(15) (a) Peerce, P. J.; Bard, A. J. *J. Electroanal. Chem.* **1980**, *114*, 89−115. b) Henning, T. P.; Bard, A. J. *J. Electrochem. Soc.* **1983**, *130*, 613−621. (c) Henning, T. P.; White, H. S.; Bard, A. J. *J. Am. Chem. Soc.* **1982**, *104*, 5862−5868. (d) Henning, T. P.; White, H. S.; Bard, A. J. *J. Am. Chem. Soc.* **1981**, *103*, 3938.
(16) Chidsey, C. E. D.; Bertozzi, C. R.; Putvinski, T. M.; Mujsce, A. M. *J. Am. Chem. Soc.* **1990**, *112*, 4301−4306.
(17) Albery, W. J.; Boutelle, M. G.; Colby, P. J.; Hillman, A. R. *J. Electroanal. Chem.* **1982**, *133*, 135−145.
(18) Gerischer, H.; Scherson, D. A. *J. Electroanal. Chem.* **1985**, *188*, 33−38.
(19) Rowe, G. K.; Creager, S. E. *Langmuir* **1991**, *7*, 2307−2312.
(20) Acevedo, D.; Abruna, H. D. *J. Phys. Chem.* **1991**, *95*, 9590−9594.
(21) Smith, C. P.; White, H. S. *Anal. Chem.* **1992**, *64*, 2398−2405.
(22) Rivera, I. M.; Cabrera, C. R. *J. Electrochem. Soc.* **1993**, *140*, L36−L38.
(23) Daschbach, J.; Blackwood, D.; Pons, J. W.; Pons, S. *J. Electroanal. Chem.* **1987**, *237*, 269−273.
(24) Bond, A. M.; McLennan, E. A.; Stojanovic, R. S.; Thomas, F. G. *Anal. Chem.* **1987**, *59*, 2853−2860.
(25) Takada, K.; Diaz, D. J.; Abruna, H. D.; Cuadrado, I.; Casado, C.; Alonso, B.; Moran, M.; Losada, J. *J. Am. Chem. Soc.* **1997**, *119*, 10763−10773.
(26) Flanagan, J. B.; Margel, S.; Bard, A. J.; Anson, F. C. *J. Am. Chem. Soc.* **1978**, *100*, 4248−4253.
(27) Peerce, P. J.; Bard, A. J. *J. Electroanal. Chem.* **1980**, *112*, 97−115.
(28) Peerce, P. J.; Bard, A. J. *J. Electroanal. Chem.* **1980**, *108*, 121−125.
(29) Merz, A.; Bard, A. J. *J. Am. Chem. Soc.* **1978**, *100*, 3222−3223.
(30) Yamada, M.; Nishihara, H. *Chem. Phys. Chem.* **2004**, *5*, 555−559.
(31) Yamada, M.; Nishihara, H. *C. R. Chim.* **2003**, *6*, 919−934.
(32) Yamada, M.; Nishihara, H. *Langmuir* **2003**, *19*, 8050−8056.
(33) Yamada, M.; Tadera, T.; Kubo, K.; Nishihara, H. *J. Phys. Chem. B* **2003**, *107*, 3703−3711.
(34) Yamada, M.; Quiros, I.; Mizutani, J.; Kubo, K.; Nishihara, H. *Phys. Chem. Chem. Phys.* **2001**, *3*, 3377−3381.
(35) Men, Y.; Kubo, K.; Kurihara, M.; Nishihara, H. *Phys. Chem. Chem. Phys.* **2001**, *3*, 3427−3430.
(36) Lenhard, J. R.; Murray, R. W. *J. Am. Chem. Soc.* **1978**, *100*, 7870−7875.
(37) Chen, S. W.; Ingram, R. S.; Hostetler, M. J.; Pietron, J. J.; Murray, R. W.; Schaaff, T. G.; Khoury, J. T.; Alvarez, M. M.; Whetten, R. L. *Science* **1998**, *280*, 2098−2101.
(38) Hicks, J. F.; Templeton, A. C.; Chen, S. W.; Sheran, K. M.; Jasti, R.; Murray, R. W.; Debord, J.; Schaaf, T. G.; Whetten, R. L. *Anal. Chem.* **1999**, *71*, 3703−3711.
(39) Ingram, R. S.; Hostetler, M. J.; Murray, R. W.; Schaaff, T. G.; Khoury, J. T.; Whetten, R. L.; Bigioni, T. P.; Guthrie, D. K.; First, P. N. *J. Am. Chem. Soc.* **1997**, *119*, 9279−9280.
(40) Chen, S. W.; Murray, R. W.; Feldberg, S. W. *J. Phys. Chem. B* **1998**, *102*, 9898−9907.
(41) Wolfe, R. L.; Murray, R. W. *Anal. Chem.* **2006**, *78*, 1167−1173.
(42) Kim, Y. G.; Garcia-Martinez, J. C.; Crooks, R. M. *Langmuir* **2005**, *21*, 5485−5491.
(43) Balasubramanian, R.; Guo, R.; Mills, A. J.; Murray, R. W. *J. Am. Chem. Soc.* **2005**, *127*, 8126−8132.
(44) Chaki, N. K.; Kakade, B.; Sharma, J.; Mahima, S.; Vijayamohanan, K. P.; Haram, S. K. *J. Appl. Phys.* **2004**, *96*, 5032−5036.
(45) Chaki, N. K.; Singh, P.; Dharmadhikari, C. V.; Vijayamohanan, K. P. *Langmuir* **2004**, *20*, 10208−10217.
(46) Quinn, B. M.; Liljeroth, P.; Ruiz, V.; Laaksonen, T.; Kontturi, K. *J. Am. Chem. Soc.* **2003**, *125*, 6644−6645.
(47) Yang, Y.; Pradhan, S.; Chen, S. *J. Am. Chem. Soc.* **2004**, *126*, 76−77.
(48) Stiles, R. L.; Balasubramanian, R.; Murray, R. W. Unpublished results, UNC-CH, 2007.
(49) Brauer, G. *Handbook of Preparative Inorganic Chemistry*; Academic Press: New York, 1965.
(50) Yu, C. J.; Wang, H.; Wan, Y. J.; Yowanto, H.; Kim, J. C.; Donilon, L. H.; Tao, C. L.; Strong, M.; Chong, Y. C. *J. Org. Chem.* **2001**, *66*, 2937−2942.

mL deionized water with 5.20 g Oct_4NBr in 200 mL toluene, gave a clear aqueous phase and an orange-brown toluene phase. Adding ω-ferrocenyl hexanethiol to the isolated organic phase (2:1 ligand-to-Au mole ratio) gave a colorless reaction mixture that was stirred for 20 min and then cooled to 0 °C. A 3.8 g portion of $NaBH_4$ in 10 mL water was added with very rapid stirring and reacted for 1 h at 0 °C, after which the dark organic phase was collected and the solvent removed on a rotary evaporator at room temperature. The black solid suspension was stirred in 400 mL of acetonitrile for 6 h, and the solid product collected and washed with acetonitrile on a fine glass frit. Determination of the average Au core size and of the number of ligands presented elsewhere[1] was based on transmission electron microscopy, UV−vis absorbance spectroscopy, cyclic and differential pulse voltammetry, and constant potential coulometry.

A mixed monolayer MPC with a lower ferrocene population (average composition, by NMR, $Au_{225}(SC6)_{58}(SC6Fc)_{17}$) was prepared by a ligand place exchange between $Au_{225}(SC6)_{75}$ (prepared as previously described[41]) and HSC6Fc at a 1:1 mole ratio of ω-ferrocenyl hexanethiol to hexanethiolate ligand. A 10-mL tetrahydrofuran solution of 0.020 g $Au_{225}(SC6)_{75}$ and 0.0089 g HSC6Fc was stirred for 1 h, the solvent removed, and the mixed monolayer MPCs rinsed with acetonitrile to remove excess thiols. The relative number of the two thiolate ligands on the exchanged product was analyzed in CD_2Cl_2 solution with ^1H NMR on a Bruker 400 MHz Avance spectrometer with a 5 s relaxation delay time.

Electrochemistry. Voltammetry of typically 0.1 mM MPC degassed CH_2Cl_2 solutions containing varying concentrations of electrolyte was done at 1.5 mm diameter Pt disk (working), Pt wire (counter), and Ag/AgCl/3 M KCl (aq) electrodes using a model 100B Bioanalytical Systems (BAS) electrochemical analyzer. The Pt working electrode was polished (0.25 μm diamond, Buehler) and cleaned electrochemically by potential cycling in 0.10 M H_2SO_4 solution. Its roughness factor (2.9) was determined from the charge under the hydrogen desorption peak in voltammetry of 0.10 M H_2SO_4, using the standard[9] 210 $\mu C/cm^2$.

The initial experiments presented will be referred to as *survey* experiments, that probe the general features of the adsorption. Freshly polished and electrochemically cleaned Pt electrodes were exposed to unstirred 0.05 mM $Au_{225}(SC6Fc)_{43}$ MPC solutions in CH_2Cl_2 containing given concentrations of $Bu_4N^+X^-$ electrolyte ($X^- = ClO_4^-$, PF_6^-, or *p*-toluene sulfonate$^-$), while cyclically scanning the electrode 25 times (0.50 V/s, total scanning time 80 s.) between 0.2 and 1.0 V (vs Ag/AgCl). The electrode was then rinsed and placed in an MPC-free solution of the same electrolyte concentration. Electrodes were also exposed to unstirred 0.05 mM MPC solutions in 1.0, 0.10, or 0.010 M Bu_4NClO_4/CH_2Cl_2 for 3 min without potential scanning (*no-scan survey*); the electrode was then rinsed with and immersed in MPC-free solutions having the same Bu_4NClO_4 concentration.

Surface coverages, Γ_{MPC} (mol MPC/cm^2), of adsorbed MPCs were calculated from the charge, Q, under the voltammetric current peaks (corrected for clean-electrode background currents) in MPC-free electrolyte solution, using

$$Q = nFA_m\Gamma_{MPC} \quad (1)$$

where n is the number of ferrocenes per MPC (average 43, by previous coulometry[1]) and A_m is the Pt electrode area corrected for roughness. The experimentally determined values of Γ_{MPC} are compared to estimates of a model MPC monolayer, based on an overall 2.4 nm MPC radius (summing Au core radius and length of the monolayer chain, including the ferrocene), that give 18.1 nm^2/MPC, or $\Gamma_{MONO,MPC} \approx 9 \times 10^{-12}$ mol MPC/cm^2.

Adsorption Kinetics. Three different protocols were employed to measure the rates of forming robustly adsorbed MPC films. In one, called the *fixed-time* kinetics experiment, a clean Pt electrode was exposed to an unstirred CH_2Cl_2 electrolyte solution containing either 1.0 M Bu_4NClO_4 or 1.0 M Bu_4NPF_6 electrolyte and one of eight different concentrations of ferrocenated MPC ranging from 0.030 to 1.0 mM. The electrode potential was cyclically scanned between 0 and 0.8 V (vs Ag/AgCl) 25 times at 0.50 V/s (a total scanning time of 80 s); the electrode was then rinsed with MPC-free 1.0 M electrolyte and placed in MPC-free 1.0 M electrolyte/CH_2Cl_2. Five preliminary CV scans at 0.10 V/s were done to remove any loosely adsorbed MPCs. Surface coverages were assessed from scans over the ferrocene wave in the MPC-free electrolyte between 0 and 0.80 V versus Ag/AgCl at six different scan rates (0.025−2.0 V/s), as described for the survey experiments, again subtracting background currents. The measured coverages were independent of potential scan rate. The Pt working electrode was then repolished, rinsed, and exposed to the next concentration of ferrocenated MPCs.

In a second adsorption-kinetics protocol, called the *no-scan kinetics* protocol, a clean Pt disk electrode was exposed at open circuit to unstirred 0.05 mM $Au_{225}(SC6Fc)_{43}$ in 1.0 M Bu_4NClO_4/CH_2Cl_2 for chosen periods of time. (The typical open circuit electrode potential was 0.2 to 0.3 V vs Ag/AgCl). The electrode was rinsed with and immersed in MPC-free 1.0 M Bu_4NClO_4/CH_2Cl_2, and Γ_{MPC} was determined by scanning over the ferrocene wave at 0.025 V/s (after preliminary scans as above). The electrode was then repolished and returned to the MPC solution for another period of (no-scan) exposure.

In the third adsorption kinetics protocol, called the *scanning kinetics* protocol, the potential of the Pt working electrode, in 0.05 mM $Au(SC6Fc)_{43}$ in 1.0 M Bu_4NClO_4/CH_2Cl_2, was cyclically scanned at 0.50 V/s between 0 and 0.80 V versus Ag/AgCl for chosen periods of time. Then the electrode was rinsed with and immersed in MPC-free 1.0 M Bu_4NClO_4/CH_2Cl_2 solution, and the surface coverage was determined as above. The electrode was then returned to the MPC solution for a further period of potential scanning time. (In this last protocol, the electrode was not polished in between exposures to the MPC solution, so the adsorption coverages represent an accumulated quantity. Several examples of doing the no-scan kinetics experiment in this way gave results agreeing with those involving polishing the electrode in between solution exposures.)

Self-Assembled Monolayer Formation. Self-assembled monolayers (SAM) of dodecanethiolate were prepared by soaking a cleaned Pt electrode for 20 h in 1 mM thiol in degassed, absolute ethanol.

Results and Discussion

Adsorption of Fully Ferrocenated Au_{225} MPCs: Survey Experiments. Cyclic voltammetry (Figure 1A−C) of 0.1 mM solutions of $Au_{225}(SC6Fc)_{43}$ MPCs in 1.0 M Bu_4NPF_6/CH_2Cl_2 shows obvious product adsorption effects; the reduction peak currents are larger than the oxidation currents. The adsorption proves to be very robust; after exposure to the MPC-containing electrolyte solution, the electrode can be removed, rinsed with MPC-free 1.0 M Bu_4NPF_6/CH_2Cl_2, and placed in MPC-free 1.0 M Bu_4NPF_6/CH_2Cl_2 to produce the very stable voltammetry shown in Figure 1D−F. The currents in the MPC-free electrolyte solution decay slightly upon initial potential scanning, but they quickly stabilize (see Supporting Information Figure S-2). The tenacity of the adsorption is illustrated by its nearly quantitative persistence after rinsing, soaking, or sonication in electrolyte-containing or electrolyte-free CH_2Cl_2; with minor variations, the same stable voltammetry (Figure 1D−F) was seen thereafter in MPC-free electrolyte solutions. The adsorbed MPCs are gradually removed by prolonged potential scanning and, naturally, by polishing the electrode. Prolonged potential scanning results, the narrowed waveshape in Figure 1D, and implied lateral attractive interactions are discussed later.

While the adsorption of the ferrocenated Au_{225} MPCs produces robust monolayers under the above circumstances, the

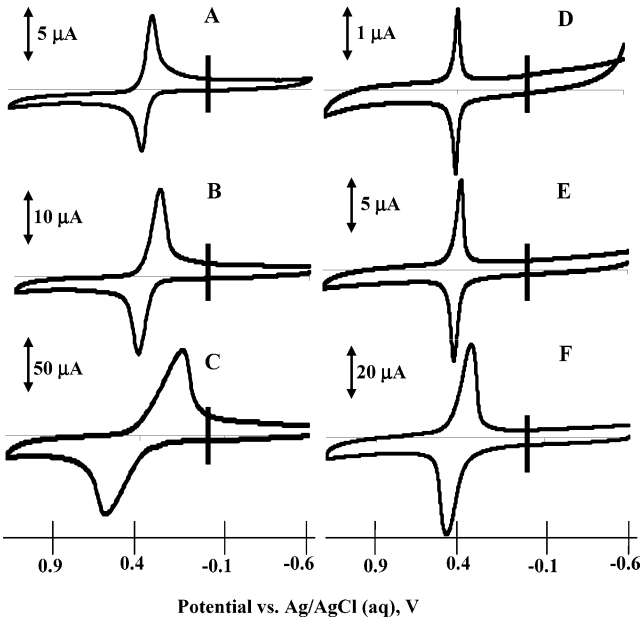

Figure 1. Cyclic voltammetry of 0.1 mM $Au_{225}(SC6Fc)_{43}$ in 1.0 M Bu_4NPF_6/CH_2Cl_2 solution at potential scan rates 0.025, 0.20, and 2.0 V/s in curves A, B, and C, respectively, and of an adsorbed $Au_{225}(SC6Fc)_{43}$ film on electrode ($\Gamma_{MPC} = 7.1 \times 10^{-12}$ mol/cm^2) formed by potential scanning in 0.1 mM MPC in 1.0 M Bu_4NPF_6/CH_2Cl_2 solution and transferred to an MPC-free 1.0 M Bu_4NPF_6/CH_2Cl_2 solution, at potential scan rates of 0.025, 0.20, and 2.0 V/s in curves D, E, and F, respectively. Results in MPC-free 1.0 M Bu_4NPF_6/CH_2Cl_2 solution at additional potential scan rates are given in Supporting Information, Figure S-1.

Table 1. Effect of Type and Concentration of Supporting Electrolyte on Coverage Γ_{MPC} of Ferrocenated MPCs Adsorbed on Pt Electrode from a 0.05 mM MPC Solution, during Potential Scanning Survey Experiment (Scan between 0.2 and 1.0 V at 0.50 V/s)

supporting electrolyte	[supporting electrolyte] M	Γ_{MPC} mol MPC/cm^2
$Bu_4NC_7H_7SO_3$	1.0	no film detected[a]
Bu_4NPF_6	1.0	6.3×10^{-12} [a]
Bu_4NClO_4	1.0	2.9×10^{-12} [a]
Bu_4NClO_4	0.10	1.4×10^{-12} [a]
Bu_4NClO_4	0.010	no film detected[a]

[a] Following rinsing and transfer to fresh electrolyte.

adsorption process is sensitive to a variety of factors, including the choice and concentration of electrolyte anion, the state of the Pt electrode surface, the population of ferrocene sites in the MPC monolayer, and whether the electrode's potential is scanned or not during exposure to MPC solution. Also, there is an uncompensated ohmic resistance associated with the adsorption that is too large to be explained by solution resistance alone. The adsorption does not appreciably change the Pt electrode double layer capacitance at potentials on the wings of the ferrocene wave. These features, the evidence for which follows, collectively point to an electrolyte anion-induced, entropically enhanced adsorption mechanism.

The extent of ferrocenated MPC adsorption, Γ_{MPC}, is strongly dependent on the particular electrolyte anion used, as shown by the surface coverage data in Table 1. The Γ_{MPC} results in Table 1, taken under *survey* experiment conditions (see Experimental) with potential scanning, are all less than the model estimate for a full MPC monolayer, ca. 9×10^{-12} mol/cm^2. This result shows that the adsorption phenomenon is not trivially

Table 2. Effect in Survey Experiments of Potential Scanning (between 0.2 and 1.0 V at 0.50 V/s), or Not Potential Scanning (i.e., Open Circuit) on Adsorption of Ferrocenated MPCs from Bu_4NClO_4/CH_2Cl_2 Solution

$[Bu_4NClO_4]$ M	Γ_{MPC} with potential scanning mol MPC/cm^2	Γ_{MPC} without potential scanning mol MPC/cm^2
1.0	2.9×10^{-12}	1.0×10^{-12}
0.10	1.4×10^{-12}	3.0×10^{-13}
0.010	no film formed	no film formed

a precipitated film; charges equivalent to many MPC monolayers were passed during potential scanning in the MPC-containing electrolyte solution (i.e., under the waves of voltammograms like Figure 1B), yet less than one monolayer is robustly retained on the electrode after rinsing and transfer to fresh electrolyte. The importance of the chosen electrolyte anion is seen by comparing results when the electrolyte is 1.0 M Bu_4NPF_6, Bu_4NClO_4, or $Bu_4NC_7H_7SO_3$. While more adsorption is seen after transfer when using Bu_4NPF_6 than with Bu_4NClO_4, *no* adsorption is seen when the electrolyte is $Bu_4NC_7H_7SO_3$.

Table 1 also shows that the adsorption is promoted by larger concentrations of electrolyte; increasing Bu_4NClO_4 concentration from 0.1 to 1.0 M in the MPC-containing solution from which adsorption is induced increases Γ_{MPC} by ca. 2-fold (as observed after transfer to MPC-free solution). Adsorption from MPC-containing 0.010 M Bu_4NClO_4 was weak and nonpersistent; the ferrocene currents dissipated quickly after a few potential scans in MPC-free 0.010 M Bu_4NClO_4/CH_2Cl_2.

While adsorption does not require scanning of potential, its amount is enhanced by scanning to positive potentials, through the ferrocene wave. Using the *survey* experiment procedure (see Experimental), clean Pt electrodes were exposed, either at open circuit (for 3 min, *no-scan survey*) or with potential scanning (see Experimental), to a 0.05 mM MPC solution of varying concentrations of Bu_4NClO_4 in CH_2Cl_2. The electrode was rinsed with and then immersed in the corresponding MPC-free electrolyte solution to assess the extent of adsorption by cyclic voltammetry. Table 2 shows that a smaller surface coverage is observed in the no-scan experiment; the resulting voltammetry is however, equally persistent in MPC-free electrolyte solution.

One may infer from the *no-scan survey* result (Table 2) that ferrocene sites need not be oxidized for robust, persistent adsorption to occur. Ferrocenated dendrimers are also known to adsorb without oxidation.[25] Also, analysis of the (narrowed) voltammetric waveshape (vide infra) is consistent with attractive lateral interactions between both oxidized and reduced absorbing nanoparticles, which would encourage adsorption. Further, a small ambient fraction of the ~43 ferrocene sites in the native MPC solution is oxidized, and cationic, given that the 0.20−0.30 V rest potentials of ferrocenated MPC solutions are not far from the ferrocene formal potential (0.40 V). Those oxidized ligand sites may aid adsorption by providing the bridging ion-pair interactions described in the ion-induced adsorption model discussed below.

The 3 min exposure in the *no-scan survey* experiments reported in Table 2 is more than sufficient (assuming $D \approx 3 \times 10^{-6}$ cm^2/s)[51] to produce a complete MPC monolayer, were adsorption to occur at a diffusion-controlled rate. (No attempt

(51) Green, S. J.; Pietron, J. J.; Stokes, J. J.; Hostetler, M. J.; Vu, H.; Wuelfing, W. P.; Murray, R. W. *Langmuir* **1998**, *14*, 5612−5619.

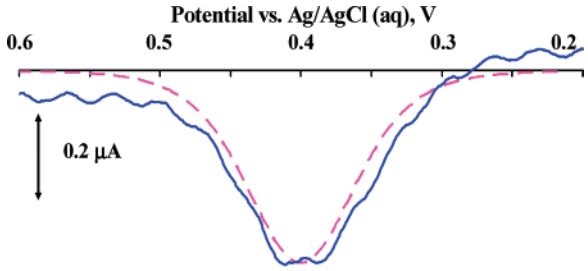

Figure 2. Oxidation peak (solid blue line) from cyclic voltammetry (2.0 V/s) of partly ferrocenated, adsorbed $Au_{225}(SC6)_{58}(SC6Fc)_{17}$ in 1.0 M Bu_4NClO_4, after transfer to MPC-free electrolyte. The dashed pink line is a simulated waveshape for a reversible one-electron transfer with no lateral interactions and with $E^{o'}$ the same for all ferrocenes (eq 3). $\Gamma_{MPC} = 2 \times 10^{-13}$ mol/cm^2.

was made to control inadvertent convective stirring.) This low coverage and the apparent irreversibility of the adsorption suggest slow kinetics of forming the robustly adsorbed film, as reported in a later section.

The ferrocenated MPC adsorption is weaker when there are fewer ferrocene sites in the MPC monolayer. Evidence for adsorption has been noticed previously[52,53] in voltammetry (in 0.10 M Bu_4NPF_6/CH_2Cl_2) of hexanethiolate-coated MPCs (average 4.8 nm core diameter) where a small fraction (10−15%) of the original thiolate ligands had been replaced (by ligand exchange) by ferrocenated ligands. Those adsorbed MPCs could be removed from the Pt electrodes simply by rinsing with fresh CH_2Cl_2 solvent. This observation was probed further here, using a higher electrolyte concentration (1.0 M Bu_4NClO_4/CH_2Cl_2) and Au_{225} MPCs bearing ca. 17 ferrocene alkanethiolate ligands (see Experimental). Figure 2 shows the oxidation peak of the cyclic voltammogram of this adsorbed MPC in MPC-free 1.0 M Bu_4NClO_4/CH_2Cl_2 solution. The surface coverage is small—about 10% of that seen in Figure 1 and less persistent than that of fully ferrocenated MPCs; the adsorption redox peaks gradually decreased during voltammetry in MPC-free electrolyte solution. Also, the Figure 2 peaks, unlike the Figure 1D−F voltammetry of adsorbed fully ferrocenated MPCs, are not narrowed and in fact show nearly ideal E_{fwhm}. These results show that the robust adsorption of Figure 1D−F is facilitated by a dense coverage of ferrocene sites on the Au MPC.

The Table 1 Γ_{MPC} results suggest that the adsorption of fully ferrocenated Au MPCs depends on specific adsorption of the electrolyte anion on the Pt surface in the CH_2Cl_2 medium. Indeed, coating the Pt electrode surface with a self-assembled monolayer (SAM) of dodecanethiolate ligands, almost completely eliminated the MPC adsorption in 1.0 M Bu_4NPF_6/CH_2Cl_2 (Figure 3).

In the course of evaluating values of Γ_{MPC}, cyclic voltammetric background currents were recorded on clean Pt electrodes in Bu_4NClO_4/CH_2Cl_2 and Bu_4NPF_6/CH_2Cl_2 solutions. Remarkably, the double-layer charging currents at potentials more positive and negative of the ferrocene wave are substantially unaffected by the ferrocenated MPC adsorption (see Figure S-3 in Supporting Information). Non-ferrocenated alkanethiolate-coated MPCs in CH_2Cl_2 solutions readily physisorb on electrodes and substantially suppress (by a factor of 2 or 3) double layer charging currents, presumably by forming a hydrocarbon-like film.[52] The adsorbed, fully ferrocenated Au_{225} MPCs are unique in our experience with MPC voltammetry in that they hardly disturb the electrode double layer capacitance. An additional implication is that small electrolyte ions can access the electrode surface through the interstices in the layer of (avg diameter near 5 nm) adsorbed MPCs.

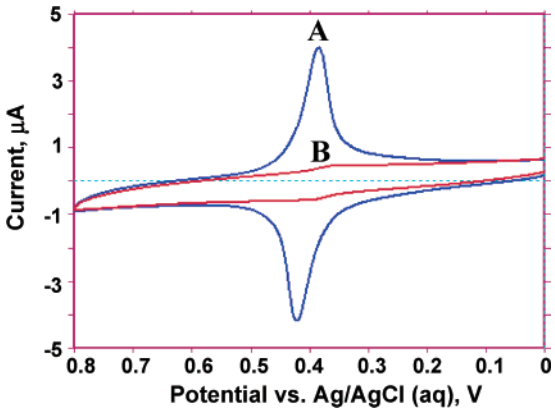

Figure 3. Cyclic voltammetry (curve A, 0.20 V/s) of an adsorbed $Au_{225}(SC6Fc)_{43}$ film formed on a clean Pt electrode from a 0.1 mM MPC, 1.0 M Bu_4NPF_6/CH_2Cl_2 solution and transferred to an MPC-free 1.0 M Bu_4NPF_6/CH_2Cl_2 solution. Curve B is the cyclic voltammetry (0.20 V/s) of an identically treated Pt electrode, except that the Pt electrode had been first coated with a dodecanethiolate self-assembled monolayer (SAM).

The longer term persistence of $Au_{225}(SC6Fc)_{43}$ MPC adsorption in MPC-free 1.0 M Bu_4NClO_4/CH_2Cl_2 was evaluated by cyclically scanning the potential of an adsorbate-coated electrode between 0.20 and 0.55 V at 0.20 V/s. Over 1840 scans of the ferrocene redox states provoked only a 16% loss in MPC coverage. On the other hand, scanning to a more negative potential limit (−0.80 V) caused a rapid decrease in Γ_{MPC} (Figure S-4); after only 280 scans Γ_{MPC} decreased *ca.* 90% of its original value. The −0.8 V limit of the voltammetric scan is more negative than the ca. −0.1 V potential of zero charge (E_{PZC}) for Pt in an organic medium.[54] The significance of this statement is that anions should be driven off the Pt electrode at such potentials, an observation in harmony with the results in Figure S-4. At the same time, we note that the MPCs are not immediately desorbed at negative potentials, which is consistent with the slow adsorption kinetics discussed later and the thus inferred lateral organization of the adsorbed film.

ΔE_{peak} values and peak-shapes in voltammograms like Figure 1D−F reveal that the adsorbed MPC layer offers a resistance to current flow. Figure 4A shows that ΔE_{peak} (at constant scan rate) increases gradually at sub- and monolayer MPC coverages. (Varied coverage is obtained in *scanning* kinetics protocol experiments, described later.) This is a defining characteristic of an uncompensated ohmic resistance effect; ΔE_{peak} should not vary with coverage (at a given scan rate) if the adsorbed layer's resistance involved slow heterogeneous electron transfers. This assignment of the adsorbed layer's resistance is supported by comparisons of experimental and simulated waveshapes (see Supporting Information Figure S-5).

Figure 4B provides a further analysis of the film's resistance, showing ΔE_{peak} versus current results at varied scan rate and constant (submonolayer) coverage (open circles). The ∼2000

(52) Miles, D. T.; Murray, R. W. *Anal. Chem.* **2003**, *75*, 1251−1257.
(53) Green, S. J.; Stokes, J. J.; Hostetler, M. J.; Pietron, J.; Murray, R. W. *J. Phys. Chem. B* **1997**, *101*, 2663−2668.
(54) (a) Marinkovic, N. S.; Hecht, M.; Loring, J. S.; Fawcett, W. R. *Electrochim. Acta* **1996**, *41*, 641−651. (b) Experimental conditions were 100 mM Et_4NClO_4/acetonitrile on Pt(100) and Pt(111) single crystals.

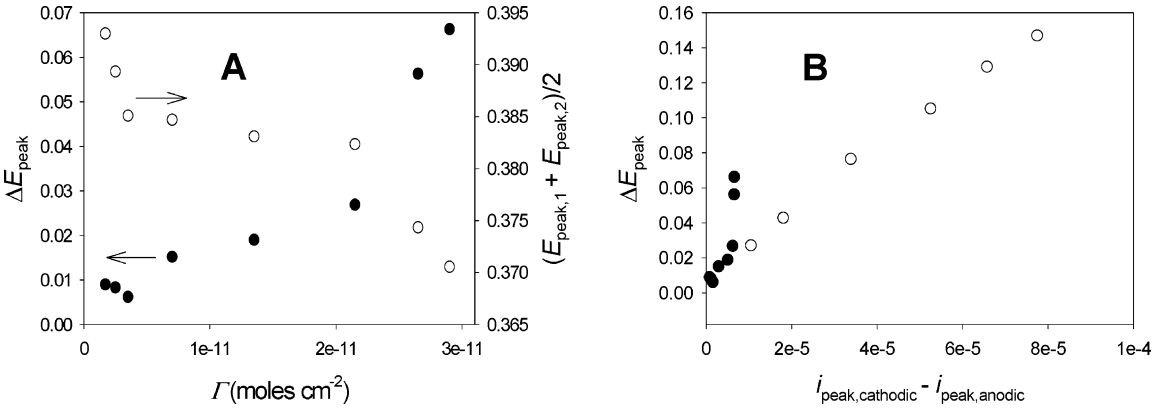

Figure 4. From cyclic voltammetry of adsorbed $Au_{225}(SC6Fc)_{43}$ films transferred to MPC-free CH_2Cl_2 electrolyte solution. Panel A: Values of peak potential splitting ΔE_{peak} and formal potential as a function of accumulated amount of robust adsorption, in 1.0 M Bu_4NClO_4 electrolyte; adsorbed films were prepared by scanning kinetic protocol. Panel B: Values of peak potential splitting ΔE_{peak} and peak current (summed oxidation and reduction) as a function of potential scan rate, from 0.025 to 2.0 V/s for films adsorbed during survey experiments like that in Figure 1D−F, in 1.0 M Bu_4NPF_6/CH_2Cl_2 solution.

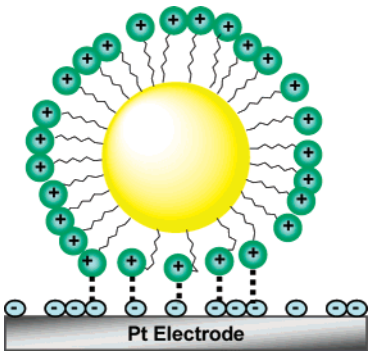

Figure 5. Cartoon of ion-induced adsorption, where ferrocenium cations on the MPC form ion-pair bridges with electrolyte anions specifically adsorbed to the Pt electrode. It can be imagined that the ligand shell may become deformed to form ion-pair bridges of similar dimensions. Formation of ion-pair bridges shown stabilizes successive ion-pair bridges and can cause a successive shift in Fc/Fc^+ formal potentials ($E_{j\max}$ scheme, see later). There may also be imagined lateral ion-pair bridges between adsorbates.

Ω total uncompensated resistance indicated by these data is consistent with the Figure S-5 simulations and is much larger than the ∼600 Ω R_{UNC} expected at a naked 1.5 mm diameter electrode. (This R_{UNC} was estimated from resistivities 188 and 156 Ω cm of 1 M Bu_4NPF_6 and Bu_4NClO_4 solutions in CH_2Cl_2 as measured by ourselves and others, respectively.)[55] It thus appears that a monolayer of robustly adsorbed MPCs offers an intrinsic ohmic resistance of the order of 1500−2000 Ω, which perhaps reflects restrained ion movement through the adsorbed layer.

While further aspects of ferrocenated MPC adsorption and its voltammetry are evaluated below, we pause here to outline how the above results suggest a mechanism for the ferrocenated MPC adsorption. We propose that it involves electrolyte anions in the electrochemical double layer forming bridging ion-pairs between the electrode and ferrocenium sites on the MPC, as cartooned in Figure 5. The persistent adsorption does not occur when the electrolyte ion (e.g., *p*-toluenesulfonate) is less structurally suited to serving as an ion bridge. Ion-pairing has been detected previously between ferrocenium and ClO_4^- and PF_6^- in aqueous voltammetry of ferrocenated SAMs,[19] in intervalent charge transfer of acetylene bridged biferrocene,[56] and in NMR[57] and QCM[22] experiments.The promotion of adsorption by scanning to positive potentials is consistent with increasing counterion adsorption as well as cationizing the nanoparticles. The present results show the importance of (a) the electrolyte anions and their concentrations, (b) their largely unchanged retention in the electrode double layer following MPC adsorption, (c) the population of ferrocene sites on the MPC, and (d) the nullifying of anion specific adsorption on the Pt surface with a hydrophobic SAM.

A likely essential aspect of Figure 5 is the *multiplicity* of the ion-pair bridges made possible by the concentrated ferrocenium population on the MPC. We propose that the strong persistence of the adsorption is at least partially due to entropic stabilization, akin to the well-known chelate effect.[58] Formation of multiple lateral ferrocenium/X^-/ferrocenium ion associations between neighbor MPC adsorbates, and of analogous ferrocene/ferrocene interactions, would further contribute to entropic stabilization and is consistent with the positive lateral interactions between neighboring adsorbed nanoparticles revealed by analysis of voltammetric waveshape (vide infra). The implied large collective ion-pair formation constants would be sensitive to the anion structure, the population of anions in the double layer, and the population of ferroceniums on the MPCs; effects all seen in the above experimental behavior. The differing Γ_{MPC} coverages in Bu_4NPF_6 and in Bu_4NClO_4 electrolytes (Table 1) may reflect differences in such details. The slow robust adsorption as well as the slow desorption are arguably indicative of kinetic slowness of adsorption and may signal some lateral ordering or organization of the MPC monolayer. Figure 5 is a nanomaterials reincarnation of the "anion-induced adsorption" model proposed many years ago by Anson, et al.[59] to account for the (much weaker) adsorption of small metal complexes on Hg electrodes.

The above phenomena are not confined to Pt surfaces and CH_2Cl_2 solvent. The persistent adsorption from CH_2Cl_2 also occurs on glassy carbon and on Au electrodes. The ferrocenated MPCs are insoluble in most electrochemically useful solvents but (much less comprehensive) tests in tetrahydrofuran showed

(55) (a) Kadish, K. M.; Ding, J. Q.; Malinski, T. *Anal. Chem.* **1984**, *56*, 1741−1744. (b) Newman, J, *J. Electrochem Soc.* **1966**, *113*, 501−502.

(56) Hupp, J. T. *Inorg. Chem.* **1990**, *29*, 5010−5012.
(57) Yang, E. S.; Chan, M. S.; Wahl, A. C. *J. Phys. Chem.* **1980**, *84*, 3094−3099.
(58) Schwarzenbach, G. *Helv. Chim. Acta* **1952**, *35*, 2344−2359.
(59) Anson, F. C.; Barclay, D. J. *Anal. Chem.* **1968**, *40*, 1791.

adsorption effects similar to those in CH_2Cl_2. MPCs adsorbed from 1.0 M Bu_4NPF_6/CH_2Cl_2 solutions could be rinsed with MPC-free 1.0 M Bu_4NPF_6/CH_2Cl_2 and placed in 1.0 M Bu_4NPF_6/CH_3CN where stable voltammetry similar to that discussed above could be observed (results not shown).

We comment that Figure 5 is based on the implicit assumption that when Γ_{MPC} coverages do not exceed the model Γ_{MPC} monolayer coverage (see Experimental), multilayers and that dendrites do not form. Reproducible observations of monolayer quantities of nanoparticle adsorption on mechanically polished surfaces over a range of experimental conditions make the latter events implausible.

Adsorption Kinetics. The slow formation of films of robustly adsorbed, fully ferrocenated Au MPCs prompted a study of their adsorption kinetics. Three different protocols (see Experimental section) were used in assessing adsorption kinetics. The *fixed-time* kinetics protocol involved exposure, while scanning the electrode potential for a fixed time, of a clean Pt electrode to either 1.0 M Bu_4NClO_4 or 1.0 M Bu_4NPF_6/CH_2Cl_2 solutions containing varied concentrations of ferrocenated MPCs. In the *no-scan kinetics* protocol, the Pt electrode was exposed at open circuit to a 0.05 mM MPC solution in 1.0 M Bu_4NClO_4/CH_2Cl_2 for varying periods of time. A third, *scanning kinetics* protocol, involved cyclically scanning the electrode potential in a 0.05 MPC/1.0 M Bu_4NClO_4/CH_2Cl_2 solution through the ferrocene wave for varying periods of time.

The results of the above experiments are displayed in Figure 6. Panel A displays the data of the *fixed-time* kinetics protocol (fixed 80 s exposure time) for the two electrolyte systems as plots of fractional coverage, $\theta = \Gamma_{MPC}/\Gamma_{SAT}$, where Γ_{SAT} is the apparent saturation (plateau) monolayer coverage, versus MPC concentration, c (lower x-axis), and versus time multiplied by concentration, tc (upper x-axis). Panel B displays MPC coverages, Γ_{MPC}, for all protocols, the *fixed-time* data of panel A, and *no-scan*, and *scanning* protocols at constant, 0.05 mM MPC concentrations, plotted versus log [tc]. Approximate adsorption rate constants can be derived from these experimental data by fitting to the first-order rate law

$$\theta = 1 - \exp(-ktc) \qquad (2)$$

where k is the adsorption rate constant, t is the time the electrode spent in the MPC solution, and c is the MPC concentration (mol/cm^3). The solid curves shown in Figure 6A,B are such fits. The corresponding rate constants for the *fixed-time* kinetics protocol are listed in Table 3. This analysis assumes that there is a maximum monolayer surface coverage, that adsorption is effectively irreversible, and that there is no concentration polarization of the MPC near the electrode. It is important to recognize that since the adsorption coverages are not true equilibrium values (any potential dependency of adsorption amount and rate is obscured by the potential scanning during adsorption), the Table 3 rate constants represent an average over the scanning potential range.

Figure 6A shows that in the *fixed-time* kinetics experiment, while Γ_{SAT} is somewhat larger in 1.0 M Bu_4NPF_6/CH_2Cl_2 ($\Gamma_{SAT} = 1.3 \times 10^{-11}$ mol/cm^2) than in 1.0 M Bu_4NClO_4/CH_2Cl_2 ($\Gamma_{SAT} = 0.7 \times 10^{-11}$ mol/cm^2), the overall rates of MPC adsorption are identical in the two electrolyte media. A single value of k (Table 3) thus serves to fit the results in both media.

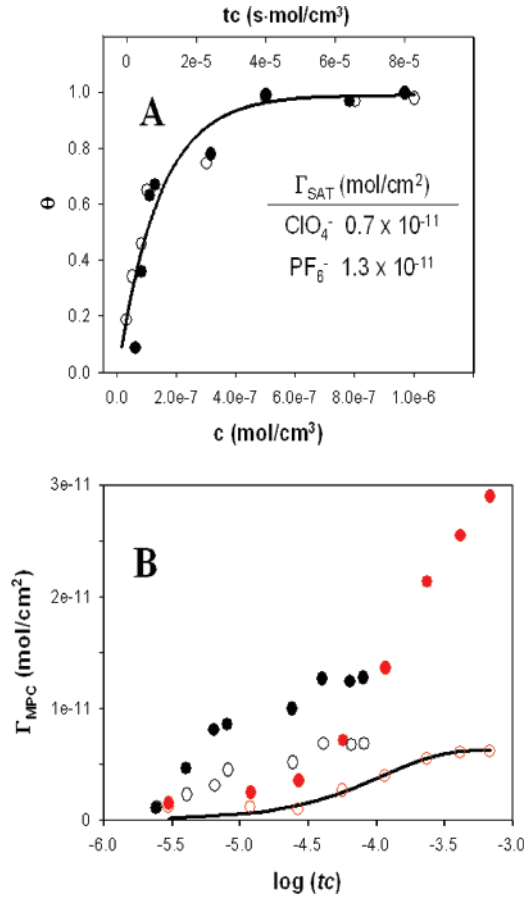

Figure 6. Panel A: Fractional coverages ($\theta = \Gamma_{MPC}/\Gamma_{SAT}$) of MPCs measured in fixed-time kinetics experiments at different MPC concentrations (lower horizontal axis) in 1.0 M Bu_4NClO_4 (open black circles, $\Gamma_{SAT} = 0.7 \times 10^{-11}$ mol/cm^2) and 1.0 M Bu_4NPF_6 (filled black circles, $\Gamma_{SAT} = 1.3 \times 10^{-11}$ mol/cm^2) electrolytes. The upper horizontal axis is normalized MPC concentration multiplied by time (tc), where $t = 80$ s for all data points. Panel B: Coverage of MPCs (Γ_{MPC}) measured as a function of log(tc) in no-scan (open red circles), scanning (filled red circles), and fixed-time (ClO_4^- filled black circles, PF_6^- circles) kinetics protocol experiments. No-scan and scanning kinetics protocols used a fixed (0.05 mM) MPC concentration in 1.0 M Bu_4NClO_4/CH_2Cl_2. The solid lines in both panels are fits to the first-order rate expression, eq 2, for the rate constants displayed in Table 3. No fit was performed on the scanning protocol as at long scanning times it led to multilayers and no obvious saturation coverage.

Table 3. Rate Constants for MPC Adsorption Derived from Fixed-Time and No-Scan Experimental Protocols[a]

experimental protocol	k, cm³/mol·s
no-scan (1.0 M Bu_4NClO_4/CH_2Cl_2)	9×10^3
fixed-time (1.0 M Bu_4NClO_4/CH_2Cl_2)	9×10^4
fixed-time (1.0 M Bu_4NPF_6/CH_2Cl_2)	9×10^4

[a] Γ_{MPC} was measured as a function of MPC concentration in fixed-time experiments and as a function of time in no-scan protocol. (All scans were taken between 0 and 0.8 V/s.)

Figure 6B plots the deposition data for all protocols as a function of tc. The open and closed black circles are the *fixed-time* kinetics data of Figure 6A. The *no-scan* kinetics results are also well-fit (open red circles, solid line) by eq 2 and produce an adsorption rate constant (Table 3) that is ca. 10-fold slower than seen in the *fixed-time* experiment (Figure 6A). This rate difference is consistent with the results of Table 2 and the model of Figure 5 and reflects the influence of scanning to positive potentials in the latter (*fixed-time*) experiment.

The results for the *scanning kinetics* protocol in Figure 6B (closed red circles) reveal an additional aspect of the ferrocenated MPC adsorption, namely that robust multi-monolayer deposition can occur given sufficiently long times (more than 3 h) of exposure to the MPC solution. The largest Γ_{MPC} attained was 2.9×10^{-11} mol/cm^2, which is equivalent to about three monolayers, and the adsorption does not appear to have reached a saturation point. From the plot, it is evident that as long as $\Gamma_{MPC} < \Gamma_{SAT}$, the rate of accumulation of Γ_{MPC} is roughly similar to that seen in the other experimental protocols, and presumably occurs with a similar rate constant. However, when $\Gamma_{MPC} > \Gamma_{MONO}$, the adsorption rate profile changes. These effects, not further analyzed here, clearly signal an increased complexity of film properties upon multilayer formation.

The voltammetry of the adsorbed ferrocenated MPCs throughout the preceding experiments continued to exhibit quite narrow peaks (like those of Figure 1D) at all monolayer or submonolayer coverages. However, when multilayers were formed in the *scanning kinetics* protocol (Figure 6B), there is (Figure 4) a small shift in formal potential and sharply increased ΔE_{peak} values (i.e., in the film's uncompensated resistance). The latter effect enhances the E_{fwhm} of the wave by ca. 2-fold, but it remains more narrow than the ideal 90.6 mV. Additionally, the behavior illustrated in Figure S-2, where a small loss of MPC coverage occurred upon preliminary potential scanning after transfer to MPC-free solution, was not seen when MPC multilayers formed.

We will return to a discussion of the possible origin of the slowness of the adsorption process later.

Voltammetric Waveshape Analysis. We turn last to the narrowed voltammetric peaks noted above for adsorbed ferrocenated MPCs (Figure 1D, $E_{fwhm} = 35$ mV). A one-electron reaction of an ideal adsorbed layer has, in contrast, a voltammetric $E_{fwhm} = 90.6$ mV and a waveshape following the equation[14,60−62]

$$i = -\frac{bF^2\Gamma_T v}{RT}\frac{\exp\left[\frac{F}{RT}(E - E^{o'})\right]}{\left(1 + \exp\left[\frac{F}{RT}(E - E^{o'})\right]\right)^2} \qquad (3)$$

where b is the number of ferrocenes per MPC, Γ_T is adsorbed MPC coverage ($\Gamma_{MPC,red} + \Gamma_{MPC,ox}$) and ν is potential scan rate. Equation 3 assumes that all redox sites react independently, have the same formal potential, $E^{o'}$, and have adsorbate activities proportional to Γ_{red} and Γ_{ox}. Equation 3 accurately represents the waveshape of dilute ferrocene monolayers as shown by the comparison in Figure 2 (pink dashed line), but for concentrated populations of ferrocene/ferrocenium sites in the MPC ligand shell, Figure 1D shows that the assumptions of eq 3 fail and narrowed voltammograms result.

We offer two alternative interpretations of the narrow voltammetric waveshape based on failures of the above assumptions. The first is a surface activity model for narrowed MPC voltammetric waveshapes that is based on attractive lateral interactions between adsorbed nanoparticles that cause activities of the adsorbates to scale nonlinearly with surface coverage.

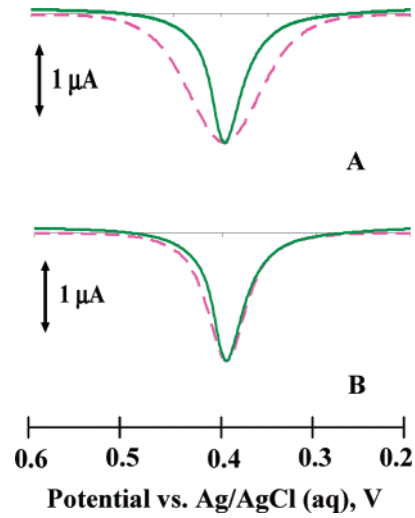

Figure 7. Ferrocene oxidation peak in experimental voltammetry (green solid line, 0.10 V/s) of ferrocenated MPCs adsorbed from a 0.1 mM MPC solution in 1.0 M Bu_4NClO_4/CH_2Cl_2 compared to waveshapes (pink dashed lines) predicted from eqs 3 (curve A) and 4 (curve B for $r_{ox} = r_{red} = 2 \times 10^{11}$ mol^{-1}cm^2). Experimental data collected from 1.0 M Bu_4PF_6/CH_2Cl_2 (not shown) gave a similarly good fit to eq 5, using $r_{ox} = r_{red} = 6 \times 10^{11}$ mol^{-1}cm^2. Predicted curves are normalized to the experimental $E^{o'}$ and peak current.

There have been several theoretical analyses[9,14,15,63−68] of how activity effects change surface waveshapes using a quantity-dependent activity, a parametrized interaction between ox and red sites, or other theoretical models.[62] A one-electron reaction, representing interaction parameters between ox and red as r_{ox} and r_{red} yields the equation[14]

$$i = -\frac{bF^2\Gamma_T \nu f(1 - f)}{RT[1 - f\Gamma_T(r_{ox} + r_{red})(1 - f)]} \qquad (4)$$

where f is the fraction of the molecules on the surface in their oxidized form. For $r_{ox} = r_{red} = 0$ (i.e., no interactions), eq 4 reduces to eq 3. The interaction parameter is signed positive and negative for attractive and repulsive interactions, respectively; attractive interactions in eq 4 lead to voltammetric peak narrowing.

Comparisons of experimental data to this model support the idea that the adsorbed layers of ferrocenated MPCs are stabilized by lateral interactions that probably involve counterion bridges that serve to screen ferrocenium charges from one another. Figure 7 compares eqs 3 and 4 (dashed pink lines, curves A and B, respectively) to MPC adsorption data (green solid lines) taken in a *survey* experiment in 1.0 M Bu_4NClO_4/CH_2Cl_2 solution. Curve A shows that the experimental oxidation peak is substantially more narrow than predicted by eq 3, while curve B shows an excellent fit for eq 4 using (quite large) attractive interaction parameters $r_{ox} = r_{red} = 2 \times 10^{11}$ mol^{-1} cm^2. Fits for eqs 3 and 4 to the experimental oxidation peak of ferrocenated MPCs in 1.0 M Bu_4NPF_6/CH_2Cl_2 (not shown) gave

(60) Laitinen, H. A.; Vincent, C. A.; Bednarsk, T. *J. Electrochem. Soc.* **1968**, *115*, 1024−1028.
(61) Laviron, E. *Bull. Soc. Chim. Fr.* **1967**, 3717−3723.
(62) Murray, R. W. *Molecular Design of Electrode Surfaces*; Wiley: New York, 1992.
(63) Chidsey, C. E. D.; Murray, R. W. *J. Phys. Chem.* **1986**, *90*, 1479−1484.
(64) Coleman, S. T.; McKinnon, W. R.; Dahn, J. R. *Phys. Rev. B* **1984**, *29*, 4147−4149.
(65) Ikeda, T.; Leidner, C. R.; Murray, R. W. *J. Electroanal. Chem.* **1982**, *138*, 343−365.
(66) Laviron, E. *J. Electroanal. Chem.* **1981**, *122*, 37−44.
(67) Ellis, D.; Eckhoff, M.; Neff, V. D. *J. Phys. Chem.* **1981**, *85*, 1225−1231.
(68) Angersteinkozlowska, H.; Klinger, J.; Conway, B. E. *J. Electroanal. Chem.* **1977**, *75*, 45−60.

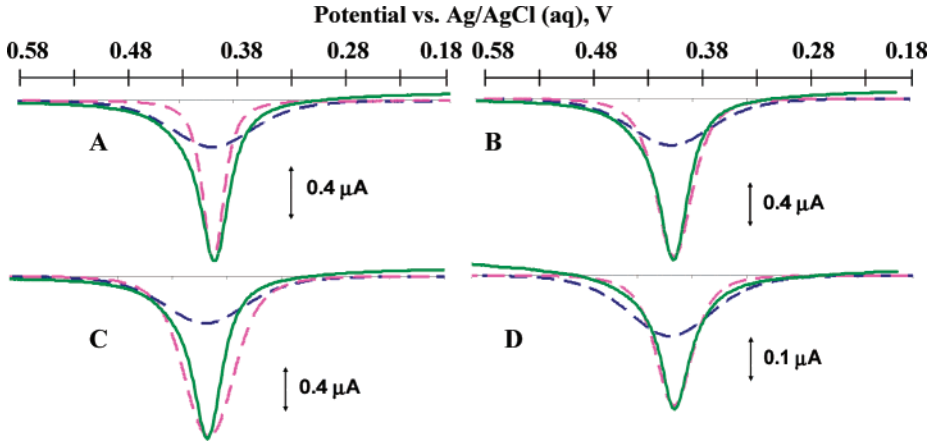

Figure 8. Simulations of the oxidative peak of a one electron transfer of an ideal adsorbed ferrocene monolayer (blue dashed line) and $E_{j\max}$ scheme with $j = 10$ and varied $\Delta E^{o'}$ (pink dashed line), compared to experimental voltammetry (green solid line, 0.025 V/s) of ferrocenated MPCs adsorbed from a 0.1 mM MPC solution in 1.0 M Bu_4NPF_6/CH_2Cl_2 (curves A−C) and 1.0 M Bu_4NClO_4/CH_2Cl_2 (curve D). Varied $\Delta E^{o'}$ fits (blue dashed line) for curve A has $\Delta E^{o'} = -1$ mV (fwhm = 23 mV), for curves B and D $\Delta E^{o'} = -4$ mV (fwhm = 35 mV), and for curve C $\Delta E^{o'} = -6$ mV (fwhm = 53 mV); the best fit for both electrolytes is at $\Delta E^{o'} = -4$ mV. To compare the curves, all are normalized to the experimental $E^{o'}$ and peak current.

identical results but required slightly larger interaction parameters ($r_{ox} = r_{red} = 6 \times 10^{11}$ mol^{-1}cm^2). These comparisons show that an activity-based model successfully represents the voltammetric peak narrowing.

Here it seems appropriate to summarize aspects of the preceding results and analyses for robustly adsorbed ferrocenated MPCs. The kinetic slowness of forming the MPC monolayers is striking and is consistent with a gradual organization of MPCs within two-dimensional films. At sub-overall-monolayer coverages, these may be small, ordered rafts. Ideas explaining slow adsorption have been discussed,[69] that include formation of ordered surface structures. Conversion of MPCs to their ferrocenium forms and lowered solubility in CH_2Cl_2, entropically driven formation of multiple ion-pair bridges to the electrode and neighbor MPCs, and the consequent strong interactions that demand organization to more stable nanoparticle arrangements must play important roles in the slow surface reaction(s). These slowly generated ordered domains on the Pt electrode may be the ones that survive solvent rinsing and transfer to MPC-free electrolyte.

A second interpretation of the narrowed voltammetric waveshapes (Figure 1D) considers that the ferrocene formal potentials are not all equal, but instead their $E^{o'}$ values gradually become less positive (by increments $\Delta E^{o'}$) as successive ferrocene sites are oxidized. The potential shift is promoted by the successive stabilization of the adsorbed ferrocenated MPC through ion-pair bridging between ferrocenium sites, electrolyte anions, the electrode, and neighbor MPCs. The cartoon in Figure 5 shows, for example, five ion-pair bridges. As each ferrocene is oxidized, consequent stabilization of the adsorbed MPC by formation of an ion-pair bridge lowers the potential for oxidation of subsequent ferrocene sites to slightly less positive $E^{o'}$. The scheme comprises $j_{\max}$ sequential reversible electron transfers ($E_{j\max}$ scheme), in which $E_j^{o'} - E_{j-1}^{o'}$ is assumed negative and constant.

In the $E_{j\max}$ scheme, each sequential electrochemical reaction is accompanied by formation of ion-pair bridges between the electrode, counteranion, and individual ferroceniums. The number of steps that involve $\Delta E^{o'}$ changes (j) is undoubtedly only a fraction of the total ca. 43 ferrocenes and may involve only those closest to the electrode (Figure 5), and perhaps next to neighbor MPCs. The reverse sequence of events occurs during reduction. Statistical aspects of many-electron-transfer reactions of redox polymers[9,26] have been presented, but do not predict peak-narrowing, and the statistical shifts of $E^{0/}$ predicted are opposite to those proposed here.

The voltammetric peak-narrowing of adsorbed MPCs in a $E_{j\max}$ scheme is illustrated in the Supporting Information in Figures S-6 and S-7, respectively, by simulations for $\Delta E^{o'} = -4$ mV and $j_{\max} = 1$ to 10 (curve 10 is thus an overall 10 electron wave) and by simulations that show the extent of peak narrowing for $j_{\max} = 10$ to be larger for smaller $\Delta E^{o'}$. While the choices of $j_{\max} = 10$ and $\Delta E^{o'} = -4$ mV to illustrate the peak narrowing effect are nominally arbitrary, Figure 8 shows that these parameters provide a good fit to the observed narrowed adsorbed MPC voltammetry in both 1.0 M Bu_4NPF_6/CH_2Cl_2 and 1.0 M Bu_4NClO_4/CH_2Cl_2 solutions (curves B, D). We do not suggest that the Figure 8 comparisons are unique, as other combinations of j and $\Delta E^{o'}$ may fit the data equally well. The main point is that a model based on progressive formation of ion-pair bridges, causing formal potential changes, can represent the peak narrowing experimental results. The $E_{j\max}$ scheme is physically appealing because it can be related to the chemical binding interactions proposed in the model for ion-induced adsorption (Figure 5). Its obvious weakness is the presumption of surface activity−concentration proportionality. It is possible that the observed peak narrowing may reflect a convolution of both of the above explanations.

It is worthwhile in closing to contrast the fully ferrocenated MPC adsorption described here to other examples of adsorption of multiferrocenated entities. A close example is that of Abruña, et al.[25] who observed significant adsorption from 0.10 M Bu_4NClO_4/CH_2Cl_2, of diaminobutane-based poly(propylene imine) dendrimers bearing 8, 32, and 64 peripheral ferrocenyl moieties. The adsorption followed a Langmuir isotherm and was strong, being observable from sub-micromolar concentrations. The voltammetric peak shapes were normal, however. A more distant comparison can be made with adsorption of poly(vinylferrocene)

(69) Zhang, J. S.; Stanforth, R. *Langmuir* **2005**, *21*, 2895−2901.

(PVF).[15,26−29] These multilayer films showed interesting complexities, including narrowed peak shapes. They have been inferred to be caused by different environments of oxidized (and reduced) sites within the film and conversions between them.

Acknowledgment. This research was supported by grants from the National Science Foundation and Office of Naval Research. Rebecca L. Stiles is the former Rebecca L. Wolfe. We thank Dr. Amala Dass for measuring the resistivity of 1 M Bu_4NPF_6 in CH_2Cl_2.

Supporting Information Available: Cyclic voltammetry of adsorbed MPCs and simulated cyclic voltammetry. This material is available free of charge via the Internet at http://pubs.acs.org.

JA074161F